THE AMERICAN SOCIETY OF MECHANICAL ENGINEERS
Three Park Avenue, New York, N.Y. 10016-5990

99-GT-43

HIGH RESOLUTION MEASUREMENTS OF LOCAL HEAT TRANSFER COEFFICIENTS BY DISCRETE HOLE FILM COOLING

S. Baldauf, A. Schulz, S. Wittig
Lehrstuhl und Institut für Thermische Strömungsmaschinen
Universität Karlsruhe (T.H.)
76128 Karlsruhe
Germany

ABSTRACT

Local heat transfer coefficients on a flat plate surface downstream a row of cylindrical ejection holes were investigated. The parameters blowing angle, hole pitch, blowing rate, and density ratio were varied in a wide range emphasizing on engine relevant conditions. A high resolution IR-thermography technique was used for measuring surface temperature fields. Local heat transfer coefficients were obtained by a Finite Element analysis. IR-determined surface temperatures and backside temperatures of the cooled testplate measured with thermocouples were applied as boundary conditions in a heat flux computation. The superposition approach was employed to obtain the heat transfer coefficient h_f referring to adiabatic wall temperatures in the presence of film cooling. Therefore, heat transfer results with different wall temperature conditions and adiabatic film cooling effectiveness results of identical flow situations (constant density ratios) were combined. Characteristic surface patterns of the locally resolved heat transfer coefficients h_f depending on the various parameters were recognized and quantified. The detailed results are used to discuss the specific local heat transfer behavior in the presence of film cooling. They also provide a base of surface data essential for the validation of the heat transfer capabilities of CFD-codes in discrete hole film cooling.

INTRODUCTION

Film cooling in combination with internal convective cooling is the common method for preventing turbine blades from excessive material temperatures. The great majority of investigations in the literature concentrate on the temperature problem of film cooling, the determination of the adiabatic film cooling effectiveness

$$\eta = \frac{T_G - T_{AW}}{T_G - T_C} \qquad (1)$$

In fact, the prediction of the material temperatures is a heat flux problem. Heat transfer from the hot gas into the wall, conduction within the wall and heat transfer from the wall to the internal cooling air flow have to be provided. Furthermore, with the internal cooling air temperature being dependent on the transferred heat flux, an iterative solution for the wall temperature has to be employed.

Especially the prediction of the heat transfer on the hot gas side in the presence of film cooling is difficult. With respect to structural and manufacturing constraints, cooling air ejection on turbine blades is restricted to discrete holes. The ejected cooling air jets induce a highly complex turbulent mixing situation, affecting the boundary layer temperature patterns as well as the local velocity profiles and, therefore, the local heat transfer coefficients. General effects of the jet and hot gas flow interaction for typical cases of inclined jets in crossflow observed by highly resolved flowfield measurements were documented by Lee et al. (1994b). Detailed flowfield measurements and additional data on the production of heat transfer enhancing turbulence by the jet ejection are provided by Pietrzyk et al. (1989, 1990), Burd et al. (1998) and Thole et al. (1998) for similar ejection situations. Highly resolved experimental data on the temperature fields responsible for the driving temperature gradients of the heat flux are given by Ryndholm (1996) and Kohli and Bogard (1997). Computational studies with highly refined grids were carried out by Sgarzi and Leboeuf (1997) for a normal ejection baseline case and by other authors, e.g. Walters and Leylek (1997), for the inclined coolant ejection. From these and other authors' investigations the basic large and small scale flowfield phenomena of inclined jets in crossflow, like jet lift off and entrainment of hot gas under the coolant jet and the resulting vortex structures, are known.

The present paper focuses on the local heat transfer coefficient, while a companion paper (Baldauf et al. 1999) treats details of the local adiabatic film cooling effectiveness. For the determination of the heat flux from the hot gas to the wall two different approaches are common. The first refers to the actual temperature of the cooling film near the wall, what would be the temperature of an adiabatic wall

$$q_W = h_f (T_{AW} - T_W) \qquad (2)$$

Herein the wall temperature independent heat transfer coefficient

Presented at the International Gas Turbine & Aeroengine Congress & Exhibition
Indianapolis, Indiana — June 7–June 10, 1999

h_f is used. The second omits the a priori unknown adiabatic wall temperature and refers to the known hot gas temperature

$$q_W = h(\theta)\,(T_G - T_W) \tag{3}$$

The influence of the actual cooling film temperature on the heat transfer in this formulation necessitates the dependence of the heat transfer coefficient on the dimensionless temperature ratio

$$\theta = \frac{T_G - T_C}{T_G - T_W} \tag{4}$$

An analysis of the simplified boundary layer equations of the convective heat transfer problem reveals a differential energy equation of a linear form for constant flow properties. Thus, a general solution can be derived from the linear superposition of two special solutions (Metzger and Fletcher 1971, Choe et al. 1974, Jones 1991). A very detailed examination of the practical relevance of the superposition approach by Gritsch et al. (1999) shows, that the linear approach is still appropriate for the range of typical temperature ratios and property variations of film cooling applications. However, conservation of an identical flow situation, particularly identical density ratio, for measurements with a variation of θ is imperative. Linearity of the problem implies both the wall temperature independence of h_f and the linearity of $h(\theta)$. For large ratios of wall to flow temperature where the flow properties within the thermal sublayer are affected, a correction of the heat transfer coefficient depending on a -0.25 power law of this temperature ratio is used (e.g. Kays and Crawford 1980). As confirmed by other authors (considerations and results of Loftus and Jones (1983), Forth et al. (1985, 1986), Teekaram et al. (1989)), for all practical purposes linearity is not greatly affected by this effect since this temperature ratio at the film cooled wall is usually close to that of the referenced unblown case. If a correction is not considered, deviations of up to 5% were stated by Teekaram et al. (1989). With the correction this deviation should disappear. Therefore, the property effects on the heat transfer coefficients are dominated by the local temperatures of the wall near cooling film that do not touch the linearity of the problem.

Since either of the two equations (2) and (3) designate the same heat flux, the use of both heat transfer coefficients is equivalent and the temperature dependent heat transfer situation summarizes as

$$h(\theta) = h_f(1 - \eta\theta) \tag{5}$$

If the heat transfer is measured in a realistic temperature ratio experiment θ is always unequal zero and the wall temperature independent h_f can not be measured directly. The only way to determine h_f is to carry out two or more experiments at different θ (where one may be an adiabatic wall experiment) and extrapolate $h_f = h(\theta=0)$ by use of Eq. (5). Result is the heat transfer coefficient h_f of the actual high density ratio flow field, comprising the property effects of this flowfield.

Investigations of the local heat transfer coefficients were performed in the vicinity of ejection holes by Kumada et al. (1981), Goldstein and Taylor (1982), Cho and Goldstein (1995) using the mass transfer analogy at unity density ratio. They provide insight into the near ejection mixing phenomena and can be related very closely to the flowfield structures described by the authors quoted earlier. Investigations extending downstream into the film region have been undertaken by Ekkad et al. (1995) and Goldstein et al. (1998), however, the local surface resolution of their results and the examined range of parameters do not allow a further interpretation of the flow situation.

The computation of jets in crossflow still suffers from problems of inadequate turbulence and wall modeling as well as from limited computational resources. Local experimental data is needed for the development and validation of refined wall and heat transfer models. The great majority of the published investigations concentrate on ejection angles of 30°-35° so that detailed data for other geometries of practical use are missing. Only few experiments were conducted at turbine like density ratios offering heat transfer coefficients appropriate for the flowfield and flow properties of the application at sufficient local resolution (e.g. Gritsch et al. 1998). Furthermore, no refined variations of flow parameters are documented that could detail the development of the coolant film flow and the lift off conditions in the high density ratio flow and subsequent effects on the heat transfer coefficients. However, highly resolved local surface data are necessary for a better understanding of the physics of the turbulent jets in hot gas flow interactions and their impact on the heat transfer coefficients.

The objective of the present study is the determination and analysis of local heat transfer coefficient distributions in the presence of high density ratio film cooling on a flat plate downstream of a row of cylindrical ejection holes. The optimization of film cooling depends on the ability to eject an adequate amount of coolant without significant augmentation of the heat transfer coefficient. Therefore, high resolution

NOMENCLATURE

α	blowing angle
D	ejection hole diameter, [m]
ε	radiative emissivity
δ_1	displacement thickness of the boundary layer, [m]
h	heat transfer coefficient, [W/m^{2}K)]
η	film cooling effectiveness, Eq. (1)
I	momentum ratio, Eq. (8)
L	ejection hole length, [m]
M	blowing rate, Eq. (6)
q	heat flux, [W/m^2]
θ	dimensionless temperature ratio, Eq. (4)
P	coolant to hot gas density ratio, Eq. (7)
ρ	density, [kg/m^3]
Re	Reynolds number
s	ejection hole spacing, [m]
σ	Stefan-Boltzmann constant, $5.67 \cdot 10^{-8}$ [W/m^{2}K^4]
T	temperature, [K]
Tu	turbulence intensity
u	velocity, [m/s]
x	streamwise coordinate, [m]
y	wall normal coordinate, [m]
z	lateral coordinate, [m]

Subscripts

AW	adiabatic wall
C	coolant
conv	convective transferred
D	hole diameter based
f	cooling film
G	hot gas
max	maximum
rad	radiative transferred
s	starting length
a	ambient
W	wall

surface data are acquired beginning close to the ejection and extending over a sufficient downstream distance. By the concentration on surface data, a substantial and systematic alteration of the parameters of primary influence could be realized to determine conditions of efficient coolant use.

Second objective of the study is the constitution of a high resolution surface data base for the validation of the heat transfer capability of CFD-codes in film cooling predictions and for the development of refined wall and turbulence models.

EXPERIMENTAL FACILITIES

The experimental method of the present investigation is based on stationary experiments in a scaled up geometry realizing engine like flow conditions. Proper temperature ratios of hot gas to cooling air are applied to obtain realistic density gradients and heat flux directions. The use of foreign gas and mass transfer analogy was avoided to exclude effects from foreign media properties.

The heat transfer measurements were carried out in an open circuit hot wind tunnel of the Institute of Thermal Turbomachinery, University of Karlsruhe. A schematic of the installation is given in Fig. 1. For a detailed description of its basic features see Baldauf et al.(1999). For the heat transfer measurements an additional cooling circuit was installed to generate a heat sink resulting in a heat flux from the hot gas into the test surface. To allow a variation of the wall temperature of the test surface, the cooling fluid temperature can be adjusted in the range of 280K to 470K. The cooling fluid used is silicon oil.

A scheme of the test section is shown in Fig. 2. The cooling air enters the test section from a plenum through cylindrical ejection holes of D=5mm diameter. The cross sectional area of the test duct is 21 x 44 D. Different ejection geometries are realized as modules that fit into the coolant plenum duct. The ejection modules are made from the semi crystalline thermoplast TECAPEK combining high thermoresistance and low thermal conductivity. They approximate an adiabatic surface at the ejection location. Effects of a coolant temperature rise in the hole passage were correlated based on the thermocouple measured plenum temperature, the blowing rate, and the hot gas temperature. The testplate connected to the ejection module extends from 2D to 82D downstream of the ejection location. It consists of 8 plates of a machinable ceramic material (Coming Macor) with a downstream length of 10D and a thickness of 2D, respectively, having a thermal conductivity of 2.0 W/mK. The plates are supported by a steal body of the same thermal expansion coefficient as the ceramic material, also bearing the connections for the cooling fluid supply. Channels are embedded below the plates to allow the direct contact of cooling fluid and ceramic. The

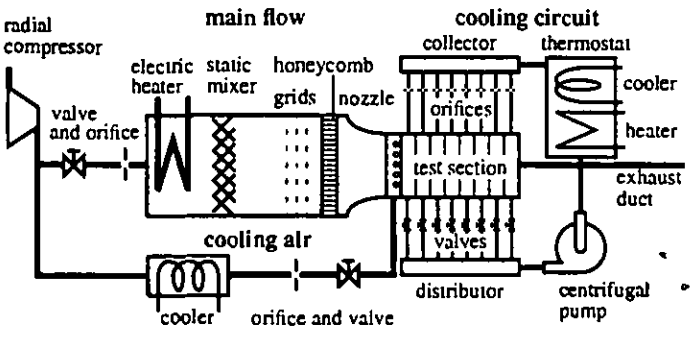

Fig. 1: Extended hot wind tunnel scheme with cooling circuit

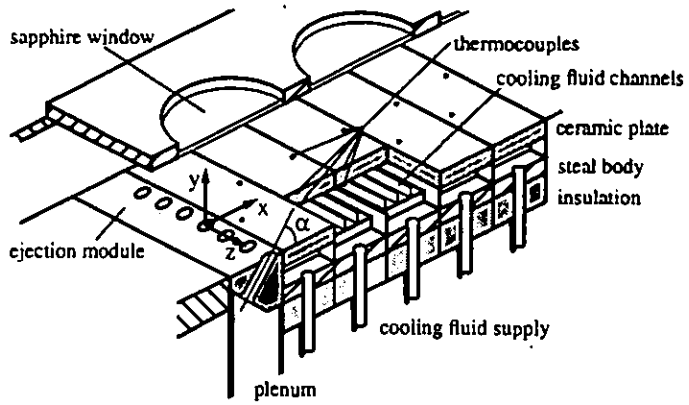

Fig. 2: Test section for heat transfer measurements

coolant fluid was applied at high flow rates resulting in very high heat transfer coefficients and a homogenous temperature on the backside of the testplate. The temperature rise of the coolant fluid crossflow was very small.

The local surface temperature measurements are performed with a high resolution IR-camera system. Ejection modules and test surface are coated with a constant emissivity dye to assure uniform radiation conditions. Two 0.25mm termocouples are mounted flush to the test surface on every segment at varying lateral positions of 2.6D to 6.1D from the channel centerline for surface temperature control and in situ calibration of the IR-camera images. A number of 5 to 8 thermocouple measurement points were used to fit the temperature processing parameters of the IR-camera images accounting for all effects of reflection of the surrounding channel temperature from the test surface as well as transmission and emission from the sapphire windows (Martiny et al. 1996). A second set of thermocouples is mounted on the cold side of the segmented testplate opposite to the surface measuring points. They allow an estimation of the heat flux at the measuring locations and were found to be sufficient to control the backside temperature boundary of the testplate. A minimum testplate thickness is needed to enable a precise distance of opposite thermocouples and the measurement of real surface temperatures. Thus, plate material and thickness were selected to realize a Biot number near unity of the regarded heat transfer process from the hot gas through the wall, to minimize the error of heat transfer coefficient determination (Jacobsen 1987).

In a test run operating point, IR-images, and thermocouple temperatures were recorded simultaneously. The accuracy of the thermocouple measurement was 0.2K, local surface temperatures on the calibrated IR-images deviated less than 1% of the actual cooling air to hot gas temperature difference. The operating conditions and examined geometries of the heat transfer measurements were the same as those of the adiabatic film cooling effectiveness measurements presented in the companion paper (Baldauf et al. 1999). Hot gas velocity was kept constant at u=60 m/s to ensure uniform velocity profile conditions at the ejection location. The cooling air temperature was kept at about T_C=300K and density ratio was adjusted by a variation of the hot gas temperature. The flow cases of the present study are specified by the dimensionless geometry and flow parameters. For every geometry and combination of blowing rate

$$M = \frac{(pu)_C}{(pu)_G} \qquad (6)$$

and density ratio

$$P = \frac{\rho_C}{\rho_G} \tag{7}$$

i.e. identical flow conditions, a set of measurements with different θ was attained by a variation of the cooling circuit temperature. In this set-up the parameter θ becomes a dimensionless wall temperature and is the result of the measurement in every point of the regarded surface. Both flow parameters blowing rate and density ratio can be combined to form the momentum ratio

$$I = \frac{(\rho u^2)_C}{(\rho u^2)_G} \tag{8}$$

The experiments were carried out in an environment of low channel background turbulence with typical large length scales to ensure that the development of important vortex phenomena of the ejection is not impeded by increased turbulent viscosity. A compilation of the dimensionless operating parameters is given in Table 1.

Table 1: Operating parameters

Geometry:	α	=	30°, 60°, 90°
	s/D	=	2, 3, 5
	L/D	=	6
Hot gas flow:	Re_D	=	6800 - 14000
	δ_1/D	=	0.1
	Tu	=	1.5%
Coolant flow:	M	=	0.2 - 2.5
	P	=	1.2, 1.8
	θ	=	1.6 - 4

DATA PROCESSING

Surface temperature data was acquired thermographically over a range of several hole pitches in the middle of the channel. The full information of a periodically uniform row of holes is contained in a stripe of 1/2 hole pitch, extending between z-normal symmetry planes in the hole center line and in the midspan. Subsequently, IR-information over several hole pitches was condensed to one half pitch stripe by averaging the temperature from the surface points of an even number of half pitches with the same streamwise coordinate and identical distance from the according centerline.

To calculate the local heat transfer coefficient following Eq. (2), the local surface heat flux is required. It was obtained by an FE-analysis of the three-dimensional internal heat flux within the testplate and ejection module, considering their different properties. The testplate was modelled as a monolithic block, interfaces between the single segments were not considered. The computational model and a typical result of this analysis is shown in Fig. 3. IR-data was applied as a temperature boundary condition on the test surface, the streamwise interpolation of the thermocouple data from the discrete measuring points on the backside of the testplate was applied to the backside of the FE-model as laterally constant temperatures. The heat transfer coefficients on the backside of the ejection module and in the ejection hole were correlated using empirical equations of Gnielinski (1975) for tube inlet flow and developing flow over a flat plate, depending on tube length and downstream distance on the surface, respectively. The complex heat transfer situation was approximated by applying the averaged heat transfer coefficients based on the mean flow velocities as a constant on the

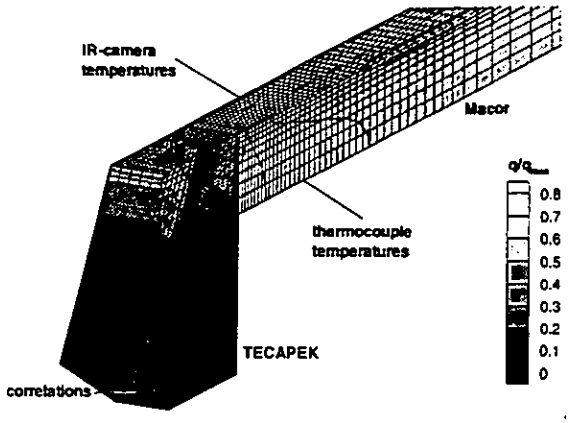

Fig. 3: FE-model of the testplate, α=60°, s/D=3

regarded surfaces, with the coolant temperature as a reference. For all other surfaces of the model adiabatic conditions were assumed.

The computation yields a precise result for the local surface heat flux q_W into the testplate as an excerpt from the three-dimensional solution. On the surface of the ejection module qualitative observations are possible and reasonable heat exchange conditions at the front end of the testplate are provided. The local surface heat flux on the testplate balances the sum of local convective heat flux and local radiative heat flux

$$q_W = q_{conv} + q_{rad} \tag{9}$$

The radiative heat transfer from the surrounding channel walls was approximated by an enclosed body approach

$$q_{rad} = \sigma \varepsilon_W \left(T_a^4 - T_W^4 \right) \tag{10}$$

where an effective local temperature T_a was applied on basis of a measured channel wall temperature. Local heat transfer coefficients h(θ) were calculated from the remaining convective heat flux for every surface data point. The surface heat transfer coefficient was normalized with the heat transfer coefficient of the unblown case, that could be well described with the empiric equation of Kays and Crawford (1980) considering an uncooled starting length x_s of the boundary layer and the temperature ratio at the wall

$$h_0 = (\rho u c_p)\, 0.03\, Re^{-0.2} Pr^{-0.67} \left[1 - \left(\frac{x_s}{x + x_s} \right)^{0.9} \right]^{-1/9} \left(\frac{T_W}{T_G} \right)^{-0.25} \tag{11}$$

The procedure of extrapolating h_f follows the linear superposition scheme described in detail by Gritsch et al. (1999) and was applied as follows:

Displayed in Fig. 4a to 4c are the surface distributions of the dimensionless temperatures from several runs at identical flow conditions, where those of the cooled surface (Fig. 4b, 4c) are processed to $h(\theta)/h_0$ data. A further local datum was taken from the adiabatic effectiveness measurement at $h(1/\eta)=0$ (Baldauf et al. 1999, Fig. 4a). In this way a minimum of three and a maximum of six single measurements at varying wall temperature conditions for every flow case were used to find the functional relation of h(θ). At every surface location, a linear regression of the points $h(1/\eta=\theta_{AW})$, $h(\theta_1)$, $h(\theta_2)$, ..., results in the appropriate values of h_f/h_0 (Fig. 4d) and η referring to Eq. (5).

It can be seen, that the junction of the ejection module and the test plate at x/D=2 introduces significant perturbations to the FE-analysis

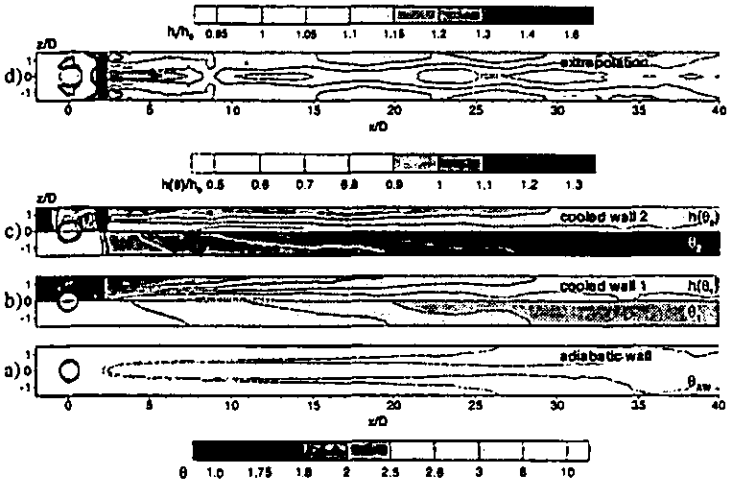

Fig. 4: Local h_f resulting from a set of surface heat transfer measurements at varying dimensionless wall temperature conditions

results, since the contact of ejection module and testplate could not be modeled perfectly. Furthermore, the single testplate segments can be detected in the result of h_f/h_0 by regular deviations of the heat transfer coefficient in streamwise direction. On the cooled testplate the accuracy of the surface heat flux computation mainly depends on the surface temperature measurement, the error of the surface heat flux is about 1%. The determination of the radiation reference temperature T_a has an error of 2%. At typical conditions, the error of the resulting heat transfer coefficient $h(\theta)$ is 3.5%, that of the extrapolated wall temperature independent normalized heat transfer coefficient h_f/h_0 is about 7%.

RESULTS

The results of the heat transfer measurements are displayed as surface contour plots of the normalized heat transfer coefficient h_f/h_0. For reasons of clarity, the actual results available for one half pitch are mirrored at the hole centerline to result in a full pitch picture. The results are presented with respect to the blowing rate as the important design parameter, the according values of the momentum ratio are also stated.

Figure 5 shows a set of heat transfer results for a shallow ejection angle, typical hole spacing, and high density ratio at the low turbulence level of 1.5%. At lower blowing rates (M=0.4 to 0.85 and I=0.09 to 0.41, respectively) typical flow conditions of a fully attached coolant jet are present. The counter rotating vortices of the coolant jet flow are lying on the surface and cause significant traces of enhanced heat transfer. These are extending from the lateral rims of the ejection hole up to about 25D downstream the ejection. By mixing and spreading of the coolant into the hot gas flow the vortices fade and the strong surface interaction diminishes. A low heat transfer region is present in the wake between and under the vortices in the centerline, where relatively low velocities are acting on the surface.

In the midspan between two ejection holes a slight decrease of the heat transfer can be stated. Since the coolant jet at the given conditions is significantly slower than the hot gas flow it is accelerated by a turbo-viscous transfer of momentum from the hot regions of high velocity close to the jet. Especially in the midspan between the coolant jets this causes a deceleration of the flow near the wall and, subsequently, a reduction of the heat transfer below the level of the unblown case. The downstream heat transfer of the very low blowing rate is slightly below the unblown case approaching unity at M=0.6 (I=0.2).

Up to M=0.85 (I=0.41) only minor changes in the vortex behavior are visible, as the vortex traces are slightly bend towards the centerline around x/D=6. The vortex surface interaction is intensified very near the ejection, but the low momentum surface patterns are still present. The vortex traces are tending towards midspan farther downstream where heat transfer is slightly augmented. The traces of adjacent jets vortices get into contact at around x/D=22 creating a stagnation line of the downwashed fluid on the surface in the midspan.

At a blowing rate of M=1.0 (I=0.56), a significant change in the flow situation can be observed. The vortex surface interaction is lost at around 7D downstream of the ejection, where the vortex traces are expected to be nearest to the centerline. Coolant flow and vortices are driven apart from the surface by the increased coolant momentum normal to the surface. Very close to the ejection hole, where the vortices have intense surface contact before they lift off, heat transfer is still intensified. The low midspan heat transfer region is filled up as could be expected from the increasing displacement effect of the ejected coolant jets (Goldstein and Taylor 1982). As a result of the increasing jet to hot gas interaction, flow turbulence is enhanced (Pietrzyk et al. 1998) and downstream heat transfer rises. With a further augmentation of the blowing rate to M=1.4 (I=1.09), the high heat transfer spots near the ejection hole move towards the centerline and merge. They form an area of combined vortex and turbulent wake heat transfer augmentation in the centerline, followed by the low heat transfer wake region. Midspan heat transfer is rising near the ejection because of the displacement effect of the coolant jets. Beginning at locations of about x/D=12 the midspan stagnation region is shifting upstream and overall heat transfer is increasing.

For blowing rates of M=1.7 (I=1.61) and beyond, a second significant change in the flow pattern takes place. Vortex interaction with the surface is suspended as the coolant jet completely detaches from the surface and penetrates into the hot gas flow. The high heat transfer area

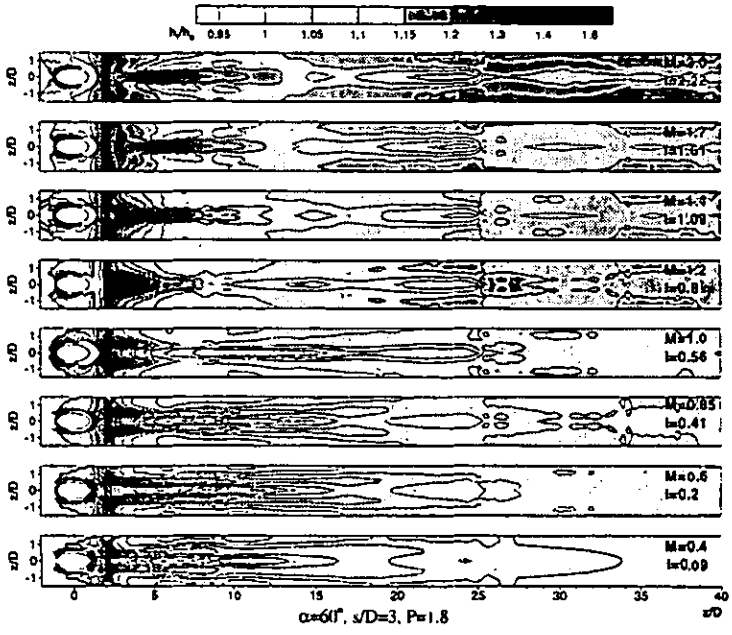

Fig. 5: Local heat transfer coefficient distributions for typical application conditions

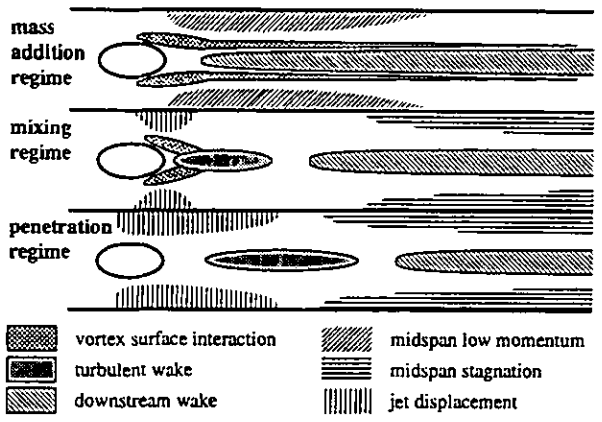

Fig. 6: Characteristic heat transfer patterns of the flow regimes for high density ratios

near the ejection hole reduces to a turbulent wake region in the centerline, extending 12D downstream. It is now separated from the ejection hole and followed by the low heat transfer wake region. The midspan stagnation region is even more pronounced and extending upstream while the midspan displacement region extends farther downstream. This situation is stable up to high blowing rates, accompanied by a further increase of the overall heat transfer coefficient ratios to around 1.2 within 50D downstream of the ejection.

A model of three different flow regimes related to the coolant surface effect and the jet lift off behavior was suggested by L'Ecuyer and Soechting (1985). The heat transfer distributions shown in Fig. 5 very precisely indicate three characteristic flow situations and confirm the model of the three regimes. The observed footprints of the mixing and lift off effects allow the allocation of specific flow behavior and resulting coolant film development. Therefore, these typical heat transfer patterns are schematized in Fig. 6 for the application relevant high density ratios and shallow angle ejection as a reference for the effects of alterations of these typical conditions.

The mass addition regime, present for blowing rates below M=1.0 or momentum ratios of I=0.5 for typical conditions, is characterized by an attached coolant jet and decreasing film temperatures with increasing blowing rates. The surface patterns are those of the flow situation that is dominated by the jet to surface interaction. The coolant jet vortices cause traces of high heat transfer separating low heat transfer areas in the midspan and in the wake region in the centerline.

The mixing regime describes the coolant jet rising from the surface with increasing blowing rate and mixing with the hot gas flow. During transition to the mixing regime the lifting jet causes coolant flow separation resulting in a turbulent wake region, emerging from the trailing edge of the ejection hole. The vortices of the coolant jet loose surface contact. Only spots of intense surface interaction at both sides of the trailing edge of the ejection hole can be found. These spots are oriented towards the centerline and merge with the turbulent wake region. The surface patterns indicate a flow situation that is governed by the jet to hot gas interaction in the vicinity of the ejection and by the interaction of adjacent jets downstream. The counter rotating vortices generate laterally alternating regions of low heat transfer in the wake on the centerline and high heat transfer on the stagnation line between the vortices of adjacent jets in the midspan.

The penetration regime is indicated by complete jet detachment and penetration into the hot gas flow, being established at M=1.7 or I=1.6 and beyond for present conditions. The vortex surface interaction at the ejection is lost as the coolant jet has completely lifted off the surface. The turbulent wake region moves downstream and separates from the ejection hole. Near the ejection the displacement effect of the coolant jet is amplified, resulting in a heat transfer augmentation. The heat transfer situation is dominated by the surface effects of the interaction of adjacent coolant jets with midspan stagnation regions and a significant centerline wake. In the following, the experimental results will be discussed according to these regimes and their typical heat transfer patterns.

In Fig. 7 the effect of steeper ejection angles on the local heat transfer is demonstrated. At low and moderate blowing rates, the coolant jet vortices do not contact the surface directly at the hole rim. Except for very low blowing rates, the coolant appears to be detached from the surface at the hole trailing edge but reattached immediately downstream.

At steep angle ejection (Fig. 7a) and low blowing rates, the vortex traces show about the same downstream extension as for shallow angle ejection. Higher turbulence production from a more intense coolant jet and hot gas interaction can be expected at the steep angle ejection, resulting in higher heat transfer coefficients. The traces begin at about x/D=3.5 after a region of very low heat transfer under the separated coolant jet. Increasing the blowing rate to M=1.0 (I=0.56), the traces are not disrupted but gradually fading and moving towards midspan where they merge and form a midspan stagnation region. The low heat transfer region near the ejection stretches further downstream in the centerline and merges with the downstream wake region indicating the reduced impact of a jet flow lifting from the surface. Starting at M=1.4 (I=1.09) typical patterns of the penetration regime are present as a separated high heat transfer turbulent wake region occurs in the centerline spreading to midspan at x/D=8. The vortex traces have moved com-

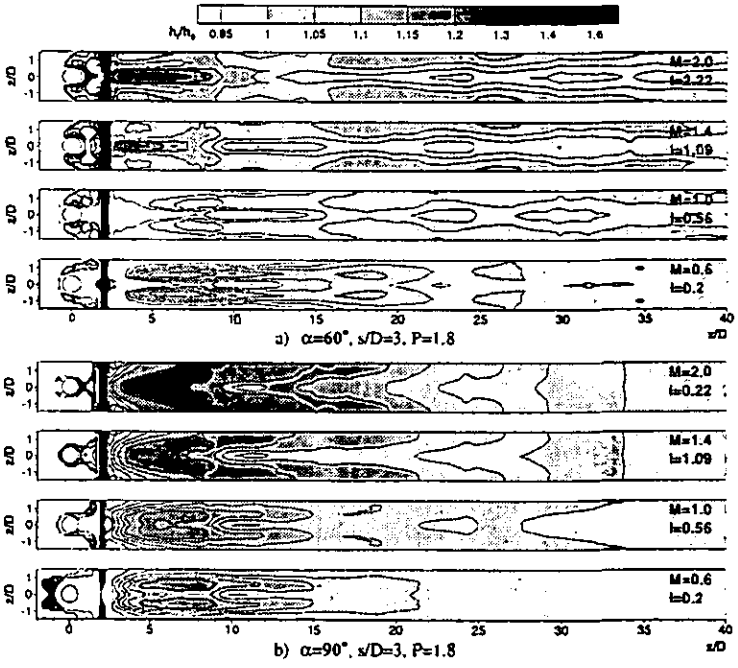

Fig. 7: Effect of the blowing angle on local heat transfer coefficient distributions

pletely to the midspan, integrating into the midspan stagnation regions at about 15D. In the midspan near the ejection the heat transfer is enhanced by the jet displacement and increasing with the blowing rate. Overall heat transfer at moderate and high blowing rates is somewhat lower than for shallow angle ejection, caused by a reduced surface interaction of the coolant jets as expected from a higher jet trajectory.

At normal injection (Fig. 7b) and low blowing rates the low heat transfer region at the ejection location is shorter. From the normal ejection situation an even more intense interaction of the hot gas flow with the coolant jets should take place causing a augmented production of jet mixing turbulence. The resulting vortex traces show higher heat transfer but also the surface flow settles at lower downstream distances. In contrast to inclined ejection, this pattern is intensifying until blowing rates of M=1.0 (I=0.56) without obvious indication of jet lift off. With increasing blowing rate (M=1.4, I=1.09 and above) the vortex traces grow together, smoothly transforming into a separated turbulent wake region that stretches over the whole span at x/D=8. The midspan stagnation region is wider and the flowfield is homogenized early around x/D=25. At high blowing rates, normal ejection produces rather spanwise than streamwise oriented patterns as expected from a vortex structured coolant flow. Beside a significant wake in the centerline very high and spanwise uniform heat transfer is found within a distance of 20D downstream of the ejection. Pronounced jet displacement effects can not be observed. With respect to the Figures 5 and 7a it can be seen from Figure 7b that the areas of highest heat transfer coefficients are confined to downstream distances of 3D to 10D with a fast decay of the values over the hole span afterwards for the normal ejection. This differs significantly from the inclined ejection, where explicit patterns of locally augmented heat transfer can be observed beyond 40D.

Figure 8 shows the influence of the hole spacing on the local heat transfer. At small pitch ejection (Fig. 8a) and low blowing rates vortex traces start near the ejection hole very close to the centerline. They are soon directed towards midspan where a pronounced stagnation region is present. Low heat transfer is found downstream in the centerline wake and at the ejection location in the midspan. At M=0.85 (I=0.41) the midspan stagnation region moves upstream, suppressing the development of the vortex traces. Close to the ejection, the interaction of the narrow spaced adjacent jets is expected to be very intense so that the early contact of the vortices with the surface is obstructed, resulting in a low heat transfer area upstream of x/D=3.5. As with the steep angle ejection, the mixing regime is bypassed over a state of very low jet to surface interaction below x/D=10 at blowing rates of about M=1.0 (I=0.56). A turbulent wake region announces the penetration regime at M=1.2 (I=0.8). This situation remains unchanged up to high blowing rates with rising overall heat transfer. The downstream situation is stable from low blowing rates up to M=2.0 (I=2.22), showing compact and intensifying midspan stagnation regions from about x/D=12 to about x/D=35. Compared to a hole spacing of s/D=3, higher overall heat transfer is induced even at low blowing rates except for the near hole region around M=1.0. At very high blowing rates of M=2.5 (I=3.47) pronounced midspan stagnation regions are induced after 3D downstream the ejection blinding out the turbulent wake region. The heat transfer coefficient ratios are rising beyond 1.5 within the first 15D and to about 1.4 within 30D downstream of the ejection. The flowfield is homogenized as soon as at a downstream distance of about x/D=25.

A completely different situation can be found for large pitch ejection (Fig. 8b). The typical vortex traces of the mass addition regime are present up to blowing rates of M=1.0 (I=0.56). They are closer to the

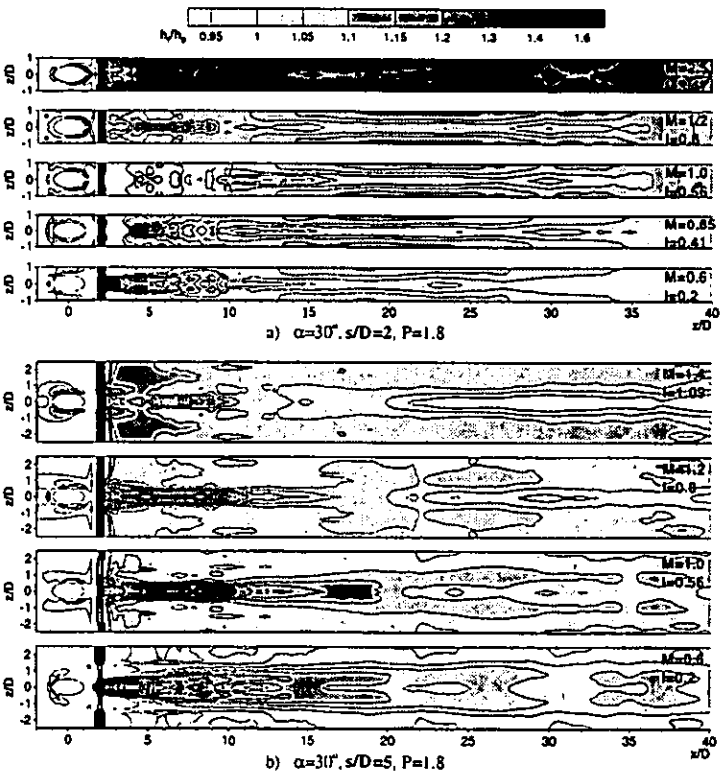

Fig. 8: Effect of the hole spacing on local heat transfer coefficient distributions

centerline and more intense than for a hole spacing of s/D=3. In contrast to the situation at smaller pitch, the traces are not interrupted and replaced by a new structure within transition to the mixing regime. They are rather growing together in the centerline forming a stretched vortex and turbulent wake region (M=1.0, 1.2; I=0.56, 0.8) followed by the low heat transfer wake. Advancing to a blowing rate of M=1.4 (I=1.09), the spots of intense vortex surface interaction move back to the ejection hole indicating that the coolant jet looses surface contact. A separated turbulent wake region of the penetration regime is left. The situation remains stable with a further augmentation of the blowing rate. The midspan region near the ejection shows gradually increasing heat transfer ratios, emerging from the ejection holes and caused by moderate jet displacement effects. Midspan heat transfer is not affected by stagnation effects for low blowing rates and at higher blowing rates only a slight increase can be found.

Figure 9 shows the effect of a reduced density ratio on the local heat transfer. For low density ratio and blowing rates up to M=0.6 (I=0.3) vortex surface traces can be detected, being less pronounced than for a high density ratio. Since coolant velocity is closer to the hot gas velocity, jet to hot gas interaction and momentum transfer to the coolant is expected to be less intense permitting a higher jet trajectory in the mass addition regime. A significant decrease of the heat transfer at midspan can not be observed. Further downstream stagnation regions are present at midspan even for low blowing rates, starting at around x/D=15. Close to the ejection, heat transfer is lower than for the high density ratio case indicating the reduced surface contact of the coolant.

At M=0.85 (I=0.6) the vortex traces have merged in the centerline forming a turbulent wake region similar to large pitch ejection, docu-

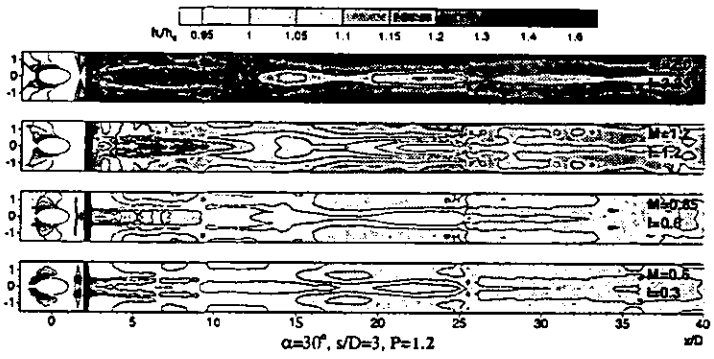

Fig. 9: Effect of the density ratio on the local heat transfer coefficient distributions

menting transition to the mixing regime. Overall heat transfer is now lower than for the high density ratio because of the higher coolant jet trajectory by the higher ejection momentum. A separated turbulent wake region can be seen at M=1.2, indicating lift off and the establishment of the penetration regime. This occurs at considerably lower blowing rate than for the high density ratio and suggests a momentum ratio of I=1.2 for the transition with typical configurations. The situation is stable up to high blowing rates with rising overall heat transfer. It is now significantly higher than for the high density ratio, as expected from an intensified turbulent mixing at the high coolant velocity of these blowing rates with respect to the high density ratio case.

DISCUSSION

In contrast to adiabatic effectiveness distributions (Baldauf et al. 1999), characteristic heat transfer surface patterns precisely denote characteristic flow regimes. Obvious changes in these patterns, displayed in Fig. 6 for typical application relevant configurations, clearly specify transitions between the different regimes. The described patterns are confirmed by observations of several authors in the near hole region (Kumada et al. 1981, Goldstein and Taylor 1982, Cho and Goldstein 1995, Gritsch et al. 1998) who provide surface heat transfer data with high local resolution. Downstream heat transfer data was not available with sufficient resolution so far. So for the first time the development of the dynamic film flow structures could be traced via the detailed heat transfer effects for a number of relevant configurations and an interpretation of the flow behavior becomes possible.

For the typical configurations the transition to the mixing regime can be expected around I=0.5 and the transition to the penetration regime around I=1.2. Important variations from the patterns for typical conditions displayed in Fig. 6 could be observed for specific combinations of the ejection parameters. For both steep angle and normal ejection, no mixing regime could be found. At steep angle ejection the mixing regime is passed by situations of very weak coolant to surface interaction around M=1.0 (I=0.56), since the surface contact of the vortices is cut off at the ejection hole. At normal ejection the flow situation seems to be governed by the turbulent jet into hot gas mixing caused by the zero downstream momentum of the coolant. Subsequently, large velocity gradients in the flowfield are present. From the heat transfer patterns can be derived that the development of compact streamwise vortices that could lift from the surface is spoiled at moderate and prevented at high blowing rates while settling of the flow is enhanced.

The downstream heat transfer patterns indicate, that the hole pitch is scaling the streamwise vortex structures of the jet flow far from the ejection location. From the surface patterns of small pitch ejection document a domination of the flow situation by intense cooling jet interaction even at low blowing rates. The development of the jet to hot gas interaction at the ejection location appears impeded. At moderate blowing rates surface structures from the jet to hot gas interaction are missing, thus, the single jet vortices do not contact the surface. Downstream, the heat transfer patterns indicate the formation of a dense and stable layer of small scaled high vorticity streamwise swirls. At large pitch ejection jet interaction seems to be merely present and flow perturbations causing heat transfer augmentation are restricted to a relatively small band in the centerline, only. According to their surface effects, the unaffected single jets very smoothly lift from the surface as the jet to hot gas interaction is freely developing and the classification into different flow regimes does not hold anymore. Penetration occurs somewhat earlier as expected from a weak jet interaction reducing the hot gas crossflow impact on the coolant jets. Lower density ratios evoke moderate velocity ratios at lower blowing rates. Surface structures similar to the large pitch ejection at higher density ratios suggest the development of the vortices farther from the surface because of a less intense jet interaction close to the ejection. Compared to the high density ratio case, higher surface normal momentum forces an earlier transition through the regimes. Downstream the effect of the interaction of the high momentum jets is more pronounced throughout all blowing rates.

In general, the observations indicate a major dependence of the single row ejection surface patterns on the two governing factors that are mixing of the coolant jet in the hot gas flow near the ejection and adjacent jet interaction downstream. Jet interaction is favored at higher blowing rates. The typical regimes, i.e. a prominent mixing regime in between the mass addition and penetration like behavior, occur as the jet interaction effects grow to the same order as the mixing effects near the ejection without one of the mechanisms getting dominant. Since this situation is present for typical applications, the interplay of both effects has to be considered for the prediction of the cooling potential of a specific configuration.

The effect of turbulence variations were not examined in this investigation. However, since hot gas turbulence is expected to mainly impact on the mixing of coolant jet and hot gas flow, the results imply how elevated turbulence levels should affect certain configurations. In situations where the flow is dominated by jet interaction effects as in the case of small pitch ejection, no significant turbulence dependence is expected. This applies also for very intense mixing situations creating excessive turbulence themselves, i.e. normal ejection. Increased turbulence is believed to have an adverse effect on the formation of compact vortex structures and to promote spreading and settling of the coolant flow, especially at low blowing rates. These assumptions are supported by a study of the turbulence effects on the flowfield by Burd at al. (1996). With respect to the unblown high turbulence case, less significant heat transfer augmentations are expected.

CONCLUSIONS

The local heat transfer coefficients downstream of a row of cylindrical holes were investigated, emphasizing application typical high density ratio conditions. A high resolution thermography system provided detailed two dimensional surface temperature data for the processing of local heat flux by a Finite Element analysis. Correction of radiation effects ensured accurate surface heat transfer coefficient data. The superposition approach was applied to sets of measurements with

identical flow parameters to extrapolate the wall temperature independent local heat transfer coefficients h_f of the high density ratio flow accounting for all effects of variable properties within the cooling film.

The local heat transfer coefficients were found to be far from the situation without coolant ejection and highly dependent on the specific blowing situation. Especially at elevated blowing rates in typical configurations a pronounced increase of the heat transfer coefficients up to 120% of the unblown reference over large downstream distances was found, what is confirmed by results of previous studies. Specific ejection parameter combinations of application relevant configurations produced an increase of more than 150% within 20 hole diameters from the ejection.

Beside general effects of heat transfer augmentation, characteristic patterns of the heat transfer coefficient distribution could be identified. Excellent observations of the jet lift off effects and mixing phenomena on the heat transfer coefficient from the present results confirm previous models and support the classification into flow regimes for typical applications. From the systematic study of these heat transfer patterns for a wide range of parameters and based on the known primary flow structures, the underlying flow behavior of specific configurations could be traced. The interpretation of the flow and mixing phenomena connected to this type of flows links results of previous detailed investigations of the ejection location and of downstream film cooling flow observations. The presented data documents significant and systematic changes in the flow behavior with the change from a shallow ejection angle to normal ejection as well as at low pitch ejection. Deviations from the characteristic behavior encountered in film cooling effectiveness examinations at these conditions could be explained.

The actual work concentrates on the flow character and its effects on the local heat transfer coefficient distributions and the mechanisms of heat transfer augmentation. The observed heat transfer patterns coincide with those of other authors. A quantitative analysis of the data is to be undertaken to enable the prediction of the heat transfer effect of discrete hole ejection on the base of laterally averaged data for design purposes. The local heat transfer coefficients together with local adiabatic effectiveness data will be used to derive local and quantitative net heat flux reduction data to identify optimum overall cooling conditions. The high resolution local heat transfer data is suited to be compared with computational results of heat flux and heat transfer coefficients in the presence of film cooling. It will be used for the validation of CFD codes for the prediction of the heat transfer to film cooled gas turbine components, as well as for the development of refined turbulence and wall models.

ACKNOWLEDGMENTS

This study was partly funded by the Ministry of Research and Technology of the Federal Republic of Germany through the German joint research program AG Turbo and Siemens AG/KWU, Mülheim a. d. Ruhr, Germany.

REFERENCES

Baldauf, S., Schulz, A., and Wittig, S., (1999). High Resolution Measurements of Local Effectiveness by Discrete Hole Film Cooling. To be presented at The International Gas Turbine and Aeroengine Congress and Exhibition, June 7-10, Indianapolis, IN.

Burd, S.W., Kaszeta, R.W., and Simon, T.W., (1996). Measurements in Film Cooling Flows: Hole L/D and Turbulence Intensity Effects. ASME Paper 96-WA/HT-7.

Cho, H.H., and Goldstein, R.J., (1995). Heat (Mass) Transfer and Film Cooling Effectiveness With Injection Through discrete Holes: Part II - On the Exposed Surface. Journal of Turbomachinery, Vol. 117, pp. 451-460.

Choe, H., Kays, W.M., and Moffat, R.J., (1974). The Superposition Approach to Film-Cooling. ASME Paper 74-WA/HT-27.

Ekkad, S.V., Zapata, D., and Han, J.C., (1997). Heat Transfer Coefficients Over a Flat Surface With Air and CO_2 Injection Through Compound Angle Holes Using a Transient Liquid Crystal Image Method. Journal of Turbomachinery, Vol. 119, pp. 580-586.

Gnielinski, V. (1975). Forschung im Ingenieurswesen 41, Nr. 1.

Goldstein, R.J., and Taylor, J.R., (1982). Mass Transfer in the Neighborhood of Jets Entering a Crossflow. Journal of Heat Transfer, Vol. 104, pp. 715-721.

Goldstein, R.J., Jin, P., and Olson, R.L., (1998). Film Cooling Effectiveness and Mass/Heat Transfer Downstream of One Row of Discrete Holes. ASME Paper 98-GT-174.

Forth, C.J.P, Loftus, P.J., and Jones, T.V., (1985). The Effect of Density Ratio on the Film Cooling of a Flat Plate. Heat Transfer and Cooling in Gas Turbines, AGARD-CP-390, Paper 10.

Forth, C.J.P and Jones, T.V., (1986). Scaling Parameters in Film Cooling. Proceedings of the 8th International Heat Transfer Conference, Vol. 3, pp. 1271-1276.

Gritsch, M., Schulz, A., and Wittig, S., (1998). Heat Transfer Coefficient Measurements of Film-Cooling Holes With Expanded Exits. ASME Paper 98-GT-28.

Gritsch, M., Baldauf, S., Martiny, M., Schulz, A., and Wittig, S., (1999). The Superposition Approach to Local Heat Transfer Coefficients in High Density Ratio Film Cooling Flows. To be presented at The International Gas Turbine and Aeroengine Congress and Exhibition, June 7-10, Indianapolis, IN.

Jacobsen, K., (1987). Experimentelle Untersuchungen zum Durchfluß und Wärmeübergang in Durchblick- und Stufenlabyrinthen. Dissertation, Institut für Thermische Strömungsmaschinen, Universität Karlsruhe.

Jones, T.V., (1991). Definition of Heat Transfer Coefficients in the Turbine Situation. Turbomachinery: Latest Developments in a Changing Scene, Paper C423/046, Proceedings of the IMechE, pp. 201-206.

Kohli, A., and Bogard, D.G., (1997). Adiabatic Effectiveness, Thermal Fields, and Velocity Fields for Film Cooling With Large Angle Ejection. Journal of Turbomachinery, Vol. 119, pp. 352-358.

Kays, W.M., and Crawford, M.E., (1980). Convective Heat and Mass Transfer. McGraw Hill, New York.

Kumada, M., Hirata, M., and Kasagi, N. (1981). Studies of a Full-Coverage Film Cooling Part 2: Measurement of Local Heat Transfer Coefficient. ASME Paper 81-GT-38.

L'Ecuyer, M.R., and Soechting, F.O., (1985). A Model for Correlating Flat Plate Film Cooling Effectiveness for Rows of Round Holes. Heat Transfer and Cooling in Gas Turbines, AGARD-CP-390, Paper 19.

Lee, S.W., Lee, J.S., and Ro, S.T., (1994). Experimental Study on the Flow Characteristic of Streamwise Inclined Jets in Crossflow on Flat Plate. Journal of Turbomachinery, Vol. 116, pp. 97-116.

Loftus, P.J., and Jones, T.V., (1983). The Effect of Temperature Ratios on the Film Cooling Process. ASME Journal of Engineering for Power, Vol. 105, pp. 615-620.

Martiny, M., Schiele, R., Gritsch, M., Schulz, A., and Wittig, S., (1996). In Situ Calibration for Quantitative Infrared Thermography. Quirt'96 Eurotherm Seminar No. 50, Stuttgart, Germany, Sept. 2-5.

Metzger, D.E., and Fletcher, D.D., (1971). Evaluation of Heat Transfer for Film-Cooled Turbine Components. Journal of Engineering for Power, Vol. 8, pp. 181-184.

Pietrzyk, J.R., Bogard, D.G., and Crawford, M.E., (1989). Hydrodynamic Measurements of Jet in Crossflow for Gas Turbine Film Cooling Applications, Journal of Turbomachinery, Vol. 111, pp. 139-145.

Pietrzyk, J.R., Bogard, D.G., and Crawford, M.E., (1990). Effect of Density Ratio on the Hydrodynamics of Film Cooling. Journal of Turbomachinery, Vol. 112, pp. 437-443.

Ryndholm, H.A., (1996). An Experimental Investigation of the Velocity and Temperature Fields of Cold Jets Injected Into a Hot Crossflow. ASME Paper 96-GT-491.

Sgarzi, O., and Leboeuf, F., (1997). Analysis of Vortices in Three-Dimensional Jets Introduced in a Cross-Flow Boundary Layer. ASME Paper 97-GT-517.

Teekaram, A.J.H., Forth, C.J.P., and Jones, T.V., (1989). The Use of Foreign Gas to Simulate the Effects of Density Ratios in Film Cooling. ASME Journal of Turbomachinery, Vol. 111, pp. 57-62.

Thole, K., Gritsch, M., Schulz, A., and Wittig, S., (1998). Flow Field Measurements for Film-Cooling Holes with Expanded Exits. ASME Journal of Turbomachinery, Vol. 120, pp. 327-336.

Walters, D.K., and Leylek, J.H., (1997). A Detailed Analysis of Film Cooling Physics Part I: Streamwise Ejection With Cylindrical Holes. ASME Paper 97-GT-269.